Deciphering *I-V* Characteristics in Molecular Electronics with the Benefit of an Analytical Model

Davood Taherinia[1] and C. Daniel Frisbie[2]

[1] Department of Chemistry, Sharif University of Technology, Tehran 11155-9516, Iran
[2] Department of Chemical Engineering and Materials Science, University of Minnesota, Minneapolis, MN 55455 USA

Abstract

We share our perspective that a simple analytical model for electron tunneling in molecular junctions can greatly aid quantitative analysis of experimental data in molecular electronics. In particular, the single-level model (SLM), derived from first principles, provides a precise prediction for the current-voltage (*I-V*) characteristics in terms of key electronic structure parameters, which in turn depend on the molecular and contact architecture. SLM analysis thus facilitates understanding of structure-property relationships and provides metrics that can be compared across different types of tunnel junctions, as we illustrate with several examples.

1. Introduction

The development of reliable approaches to electrically contact single molecules and molecular assemblies over the last 20-25 years has resulted in a broad spectrum of intriguing discoveries.[1–11] Researchers now build metal-molecule-metal junctions that exhibit a range of behaviors, including current rectification,[12–15] switching,[16–18] photoconductivity,[19–21] magnetoresistance,[22–24] and negative differential resistance[25–27] that may hold promise for future nanotechnologies. These milestones reflect both technical advances in molecular junction formation and increased understanding of fundamental structure-property relationships in the field of molecular electronics.

Despite recent progress, there is still much we don't understand regarding the conductance of molecules, even simple ones, connected to metal contacts, **Figure 1A**. One can ask: What should the current-voltage (*I-V*) curve look like for a molecule? Or more specifically, what is the functional dependence of *I* on *V* and can we predict how it depends on the contacts, or molecular length, or chemical substitution, symmetry, and bond architecture? Many decades ago similar structure-function questions were asked about semiconductor junctions. The path forward in semiconductor electronics was to understand electronic structure, specifically the electronic density of states (or DOS) and its behavior under applied bias for different device architectures. The same strategy applies to molecular electronics, and this is the focus of many researchers in the community.[28–34]

In this context, the main point of this Perspective article is to highlight that an analytical model, derived from first principles, is a useful and easily accessible tool for relating *I-V* characteristics to electronic structure for simple molecular tunnel junctions. We will not focus here on many of the exciting phenomena mentioned above associated with complex molecular junctions; our intent here is to make sure we understand what happens in simple cases. In doing so, our discussion will highlight the benefits of having an analytical model, namely that it facilitates fundamental understanding of the underlying physics, that it enhances quantitative interpretation of *I-V*

behavior, and that it provides metrics that can be compared across different molecular architectures. Enhancing quantitative analysis of molecular junction behavior is an important goal for molecular electronics as it develops as a thriving sub-discipline of chemistry and physics.

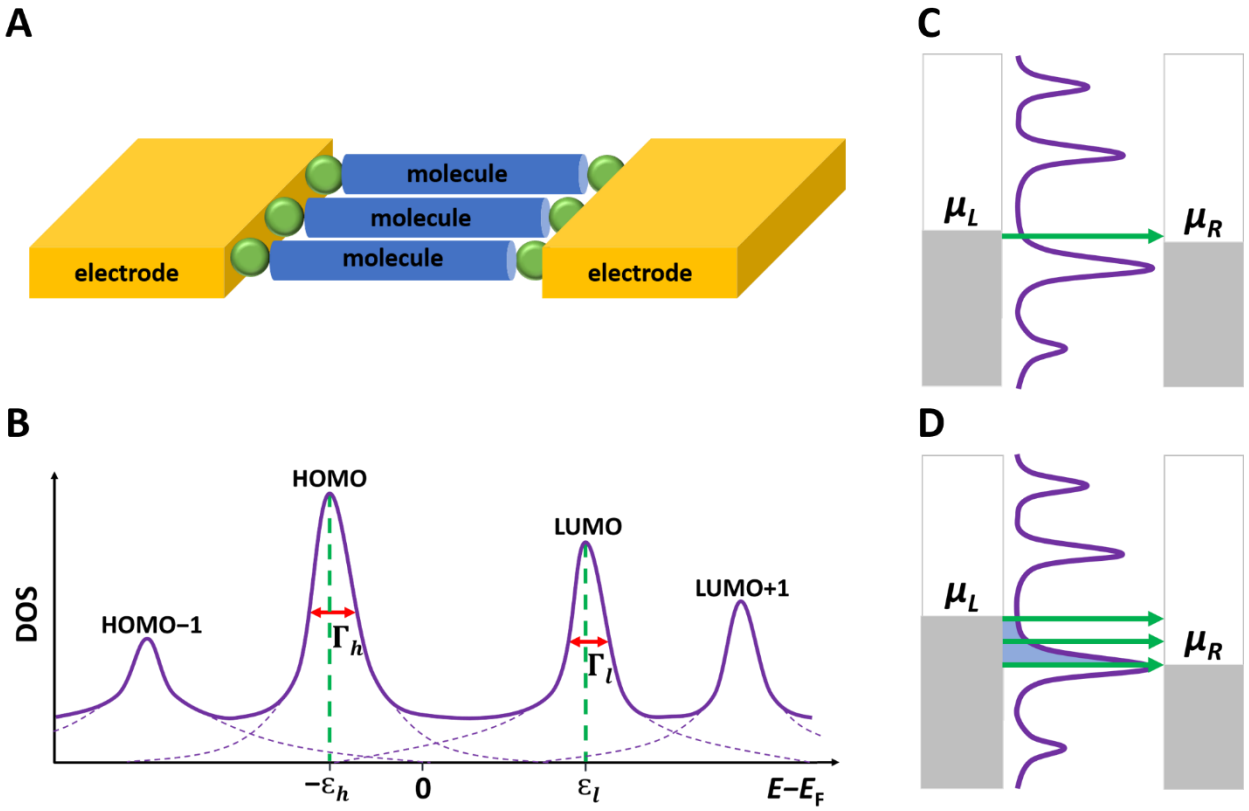

Figure 1. (A) Schematic representation of a molecular junction. (B) A generic scheme of the DOS for a molecular junction. (C) Off-resonant tunneling at E_F upon the application of a small bias between the two electrodes. (D) Opening an "energy window" in the DOS (shaded in blue) upon the application of a large bias between the two electrodes. The green arrows in panels C and D indicate the direction of electron flow.

2. Molecular Conductance, Junction Electronic Structure, and the Single-Level Model

A generic scheme of the DOS for a molecular junction is shown in **Figure 1B**. Two occupied orbitals (HOMO and HOMO – 1) and two unoccupied orbitals (LUMO and LUMO + 1) are shown and the Fermi level E_F of the junction lies in this case closest to the HOMO. The widths of the orbitals are broadened due to interactions with neighboring molecules and with the metal electrodes; it is often assumed that the broadened lineshapes are Lorentzian.[35] For tiny applied biases between the metal contacts, off-resonant electron tunneling will occur at E_F, **Figure 1C**.[36] "Off-resonant" simply implies that the peak of the facilitating orbital, in this case HOMO, is shifted from E_F. Electrode-to-electrode tunneling is resonant with orbital states in the "tail" of the HOMO distribution that are aligned with E_F. These are the states that the tunneling electron couples to as it crosses the junction. Note that the DOS at E_F includes contributions from the tails of all the orbitals, especially those nearest E_F. We will return to this point in section 5.

Application of a larger voltage between the two metal contacts opens up the "energy window" in the DOS in which electrode-to-electrode (direct) tunneling will occur, **Figure 1D**. The Landauer-

Buttiker formalism ("conduction is transmission") provides a way to calculate the resulting current[37–39]:

$$I = \frac{2e}{h}\int_{-\infty}^{\infty} T(\varepsilon)[f_L(\varepsilon - \mu_L) - f_R(\varepsilon - \mu_R)]d\varepsilon \qquad (1)$$

where I is the total tunneling current through a single molecule junction, e is the electron charge, h is Planck's constant, μ_L and μ_R are the electrochemical potentials (Fermi levels) of the left and right electrodes, ε is electron energy, f_L and f_R are the Fermi distribution functions of the left and right electrodes, and $T(\varepsilon)$ is the transmission function. Note that the applied bias $V = (\mu_R - \mu_L)/e$. The transmission function $T(\varepsilon)$ is a dimensionless number between 0 and 1 that represents the probability of quantum mechanical tunneling at a given energy ε. Importantly, $T(\varepsilon)$ is directly proportional to the junction DOS at ε, i.e., $T(\varepsilon) \propto \mathrm{DOS}(\varepsilon)$.[40] Thus, the larger the DOS in the energy window, the higher $T(\varepsilon)$ will be and thus the larger the tunneling current.

$T(\varepsilon)$ is not generally known to the experimentalist, nor is the DOS, except perhaps in a qualitative sense. In fact, a desirable goal for the experimentalist is to use the measured *I-V* characteristics to determine the DOS and $T(\varepsilon)$! The DOS and $T(\varepsilon)$ can then be related to structure, i.e., the molecular length and bond architecture, the type of metal-molecule contact chemistry, the contact metal type, and so on. The electronic structure is the link between the molecular junction architecture and the measured *I-V* behavior.

So how can the DOS and $T(\varepsilon)$ be determined from the *I-V* characteristics? A common way in the literature is a computationally demanding approach in which a certain structure for the junction is assumed (or computed), and density functional theory (or DFT) is employed to then calculate $T(\varepsilon)$ and the *I-V* behavior using Equation 1.[41–44] Mismatch between the computed *I-V* and the measured *I-V* can then guide computational iterations in which the structure of the junction is changed, $T(\varepsilon)$ is recomputed, and the *I-V* is recomputed until there is an acceptable level of convergence. This approach is widely employed but it is time-consuming and requires expertise that most experimental groups do not have. Collaboration between experimental and DFT research groups provides a solution, but it is also highly desirable to have a model that is readily accessible to the experimentalist, one in which the assumptions and results are more transparent to the non-expert.

Thus, our desire is to reduce the computational burden considerably and to have an accessible analytical model that relates the measured *I-V* characteristics quantitatively to the DOS and $T(\varepsilon)$ for a particular junction. The Single-Level Model (SLM) accomplishes this in the limit of certain assumptions that turn out to be valid for many simple tunneling junctions,[35,45] as we will discuss below. The first assumption is that only the orbital nearest E_F (HOMO or LUMO) is important for tunneling. We will soften this assumption for the case of low bias, as discussed in section 5, but for now we proceed with the idea that only one orbital matters. **Figure 2** displays a simplified DOS in which only the HOMO is shown. Its position in energy is characterized by the HOMO-to-Fermi level offset, ε_h. The second assumption is that the shape of the HOMO, which is due primarily to

metal-orbital coupling, is Lorentzian and characterized by a width Γ. With these assumptions the transmission $T(\varepsilon)$ is given by the Breit-Wigner formula:[46]

$$T(\varepsilon) = \frac{\Gamma^2}{(\varepsilon-\varepsilon_h)^2+\Gamma^2} \qquad (2)$$

Using this expression for $T(\varepsilon)$, and in the zero temperature limit, eq. 1 can be integrated analytically to give:

$$I = N\frac{G_0}{e}\frac{\Gamma^2}{\Gamma_a}\left[tan^{-1}\left(\frac{\varepsilon_h+\frac{eV}{2}}{\Gamma_a}\right) - tan^{-1}\left(\frac{\varepsilon_h-\frac{eV}{2}}{\Gamma_a}\right)\right] \qquad (3)$$

where N is the number of molecules in the junction (the number of parallel conduction channels), $\Gamma = \sqrt{\Gamma_L\Gamma_R}$ is the geometric mean of the orbital couplings Γ_L, Γ_R to the left and right electrodes ($\Gamma_L \approx \Gamma_R$ in symmetric junctions), $\Gamma_a = \frac{\Gamma_L+\Gamma_R}{2}$ is the arithmetic mean of $\Gamma_L$and Γ_R, and $G_0 = 2e^2/h$ is the conductance quantum.

The single-level formu la in eq. 3 is also often called the resonant tunneling model because it predicts that current plateaus at large voltages where resonant transport through the HOMO (or LUMO) becomes possible (see Figure 1D). Eq. 3 is still a bit cumbersome in our view and further simplications can be made. In particular, for self-assembled monolayer (SAM) based junctions emphasized here, resonant current plateaus are rarely seen; tunneling is usually decidedly off-resonant. To express the off-resonance condition, we take $\Gamma << \varepsilon_h$ and $V \leq 1.4\ \varepsilon_h$. With these additional assumptions, Baldea has shown[35] that eq 3 can be simplified to a new analytical equation for direct metal-to-metal, single step, off-resonant tunneling in a molecular junction:

$$I = GV\frac{\varepsilon_h^2}{\varepsilon_h^2-(eV/2)^2} \qquad (4)$$

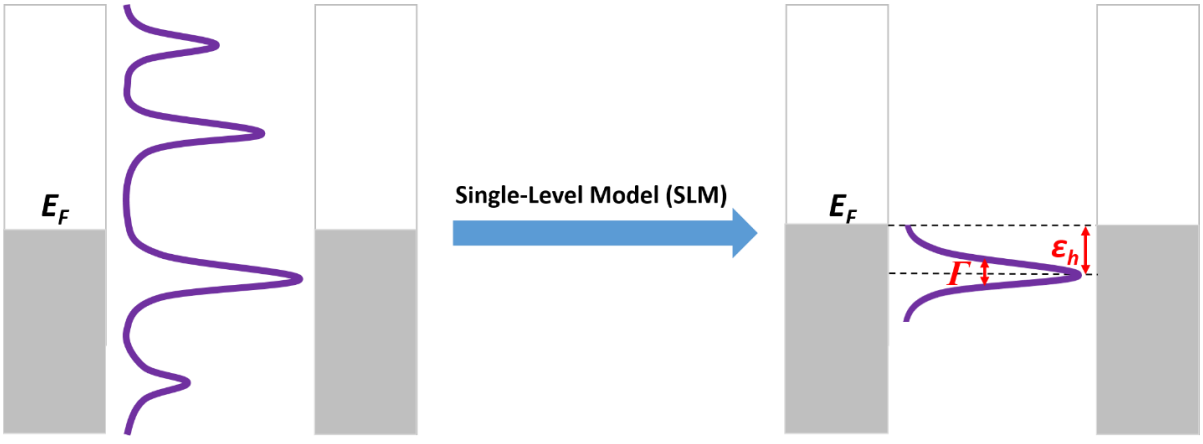

Figure 2. A simplified electronic structure of the molecular junction (right) along with the key parameters ε_h and Γ, obtained from the actual DOS (left) under the assumptions of the SLM.

where the low bias conductance G of the junction is given by

$$G = NG_0 \frac{\Gamma^2}{\varepsilon_h^2} \qquad (5)$$

Interestingly, the bias voltage V appears in two places in eq. 4. At low bias voltages, the V^2 term is negligible compared to ε_h^2, and eq. 4 reduces to

$$I = GV = NG_0 \frac{\Gamma^2}{\varepsilon_h^2} V \qquad (6)$$

That is, at low bias I is *linear* in V and $T(\varepsilon) = N\frac{\Gamma^2}{\varepsilon_h^2}$. At high biases, the V^2 term in the denominator of eq. 4 is important and the current has a distinctly non-linear behavior with increasing V. Typical I-V curves appear almost parabolic in the high bias regime, **Figure 3A**, but are clearly linear in the low bias regime. It should be understood that the V^2 dependence in eq. 4 is a natural consequence of the Lorentzian shape of the HOMO and the fact that as V increases, the tunneling experiment is sampling more and more of the HOMO lineshape and getting closer to resonance, **Figure 1D**. At low V values, on the other hand, the tunneling occurs in the trough of the DOS, relatively far away from the HOMO peak.

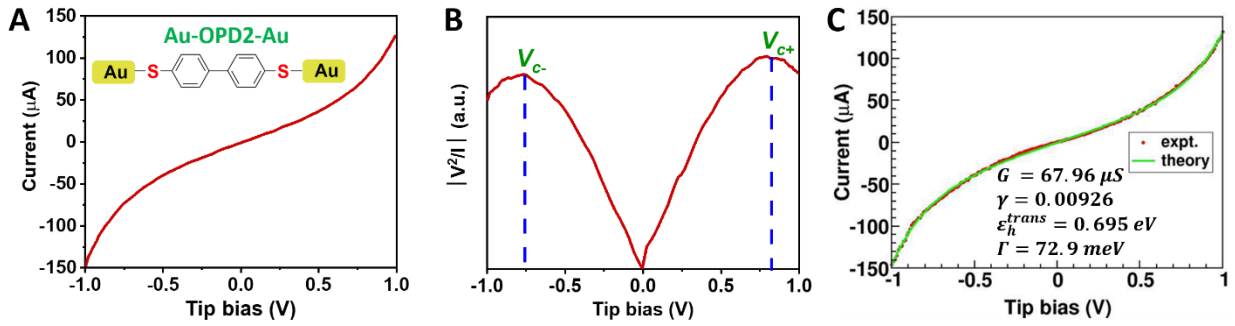

Figure 3. (A) A typical experimental I-V curve and (B) the corresponding $|V^2/I|$ vs V plot obtained for an Au-OPD2-Au CP-AFM molecular junction. (C) The theoretical I-V curve calculated according to the SLM (green curve) along with the experimental data (red curve). Adapted with permission from Ref. 47. Copyright 2015 American Chemical Society.

We emphasize that the original single-level formula in eq. 3 also describes off-resonant I-V behavior, as in Figure 3a, but eq. 4 shows the functional dependence of I on V more clearly and the overall equation is simpler. As we will show, the form of eq. 4 has allowed insights into off-resonant behavior that were previously missed. Importantly, either eqs. 3 or 4 can be used to produce high quality fits to the experimental I-V data for off-resonant transport, but our preference from this point forward will be to use the Baldea equation, eq. 4.[45,47–50] The fitting parameters are the low bias conductance G and the orbital energy offset ε_h, just two parameters. If the number of molecules in the junction N is known, then one can also determine Γ from eq. 5, and the fit produces the two fundamental parameters, ε_h and Γ, characterizing the electronic structure as shown in **Figure 2**.

We must introduce one important modification to eq. 4 (and this would also apply to eq. 3). If the facilitating orbital (HOMO in this discussion) is not spatially centered in the junction (i.e., the HOMO probability distribution is nearer one electrode), then its energy will also be a function of V, and the orbital energy will shift up or down depending on the magnitude and sign of V.[35,49,51] This is an electrostatic effect: the electrons in the orbital feel the electric potential (or the field) in the junction. This potential is partially screened by the dielectric response of the molecules, but the screening is not perfect and thus there is an electric potential drop (and an associated electric field) across the molecules, **Figure 4A**. If the orbital is perfectly centered in the junction, then (in the absence of a Stark effect), there is no shift of the orbital energy. However, if the orbital is off-center, its energy will track the potential on the closest electrode, **Figure 4B**. To account for this electrostatic effect on the orbital energy offset, the orbital shift factor γ is introduced,

$$\varepsilon_h(V) = \varepsilon_h + \gamma eV \qquad (7)$$

where ε_h is the HOMO energy at zero bias. Equation 7 says that the orbital energy will shift with applied bias V, and how much it shifts and which direction are determined by the magnitude and sign of γ. Now we can modify eq. 4 to take account of this effect:

$$I = GV \frac{\varepsilon_h^2}{(\varepsilon_h+\gamma eV)^2-(eV/2)^2} \qquad (8)$$

Here again $G = NG_0 \frac{\Gamma^2}{\varepsilon_h^2}$, as shown in eq. 5. Eq. 8 is the complete analytical single-level model (the "Baldea Equation") for simple off-resonant tunneling junctions. It has three fitting parameters: ε_h, G, and γ. The number of fitting parameters reduces to two, ε_h and G, when the junction is symmetric and γ is negligible (eq. 4). In the next section we discuss how we extract these parameters in a way that is most consistent with the data; we do not treat each parameter as freely adjustable. We emphasize that it is important to remember the assumptions underlying the SLM described above, so that the SLM is not applied to *I-V* analysis in cases where those assumptions are violated.

3. Analysis of *I-V* Data with the Single-Level Model

As mentioned above, **Figure 3A** shows a typical experimental *I-V* curve for a molecular junction based on an oligophenylene dithiol (OPD2).[47] The junction was made by forming a self-assembled monolayer (SAM) of OPD2 molecules on a flat, template-stripped gold substrate.[47] The second contact was made using a gold-coated atomic force microscopy (AFM) tip. This type of junction, commonly made in our laboratory, is not a single molecule junction, but rather it is an ensemble of 60-70 parallel molecules. The number of molecules is estimated from the measured molecular surface coverage and the tip-SAM contact area, which is measured to be ~25 nm^2.[52]

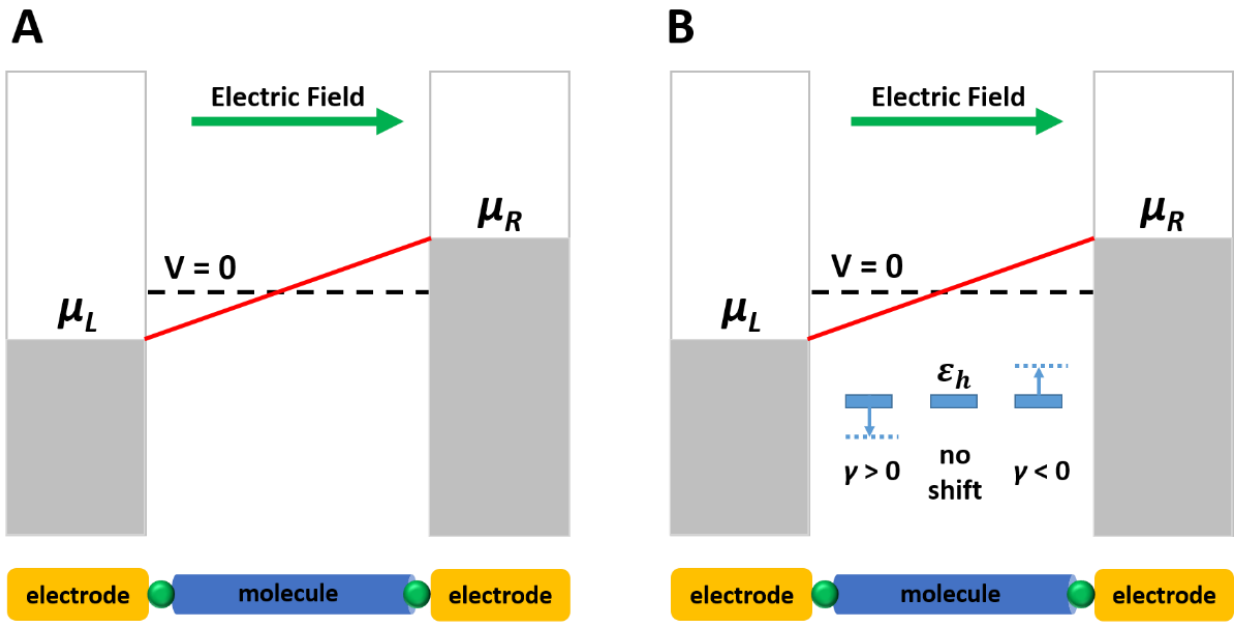

Figure 4. (A) A simplified potential profile (red line) across the molecular junction in the presence of an applied bias. (B) Illustration of the voltage-driven HOMO-level shifting and the shift factor γ based on the spatial location of the HOMO electron probability density.

A systematic approach is followed to determine the best fit of the data to eq. 8. First, the value of low bias conductance G is determined by considering only a very small voltage window around 0 V, say ± 0.1 V. A straight line fit to $I = GV$ (eq. 6) gives G (the same G as in eq. 8). To determine ε_h, we find the voltage corresponding to the maximum in a plot of $|V^2/I|$ vs V, **Figure 3B**. The function V^2/I is a convenience function, i.e., it does not have specific physical meaning, but it is a function that can be readily calculated from the data and its maximum occurs at a voltage V_c that can be quantitatively related to ε_h. You can think of V_c as a characteristic voltage of the system that is a measure of when the I-V curves become significantly non-linear (it is easy to show that at $V=V_c$ the nominal conductance I/V is equal to $2G$). For historical reasons, one will also see this characteristic voltage described as V_t, or 'transition voltage'.[35,53] Importantly, Baldea[35] has shown that,

$$eV_c = 2\varepsilon_h/\sqrt{3} \qquad (9)$$

Other convenience functions could be chosen, but V^2/I is the one we typically employ. So, from the $|V^2/I|$ vs V plot, we obtain the characteristic voltage V_c, and from eq. 9 we have ε_h. Plugging G and ε_h into eq. 8 gives the fit, as shown in **Figure 3C**. If there is any asymmetry in the I-V characteristic, this can be accommodated by adjusting γ. The quality of the fit can of course be quantitatively assessed by calculating the mean squared error, and small adjustments in ε_h and γ can be made to minimize the error. Typically, we do not adjust low-bias G as the linear fit for G around 0 V has little ambiguity. Technically, the fit of eq. 8 to the data is a three-parameter fit, but we emphasize that these parameters are not freely adjustable; they have clear constraints. In most cases (e.g., **Figure 4**), where γ is very small or zero, one can view the fit as essentially a one-parameter fit for ε_h, as the fit for G is quite prescribed.

With G, ε_h, and γ in hand, the last step is to estimate Γ using eq. 5. A required input is N, the number of molecules in the junction. For conducting probe atomic force microscopy (CP-AFM) junctions this is typically known to within ±10%[52] and thus the calculated Γ will have a confidence interval that reflects the uncertainty in Γ, which is proportional to $\sqrt{N}$. If N is not known, then Γ cannot be determined. But even in that case the SLM still has value as it provides ε_h and γ, which are independent of N.

4. Successful Applications of the Single-Level Model

4A. Demonstration of the correspondence of ε_h^{trans} with ε_h^{UPS} determined by ultraviolet photoelectron spectroscopy (UPS). One of the most important recent successes of the SLM analysis with the Baldea equation has been verification that the ε_h values extracted from the transport data closely match the values of ε_h determined independently by ultraviolet photoelectron spectroscopy (UPS).[54,55] In UPS, irradiation of a sample with ultraviolet light causes emission of valence electrons by the photoelectric effect; kinetic energy analysis of the photoelectrons produces a spectrum of electron count versus binding energy of the occupied valence electronic states. From these measurements one can measure the HOMO energy of a SAM with respect to the Fermi level of the substrate metal. We call this HOMO energy ε_h^{UPS}. Because UPS is a well-established surface science technique, it was important to us to compare the results for ε_h obtained from tunneling and UPS.

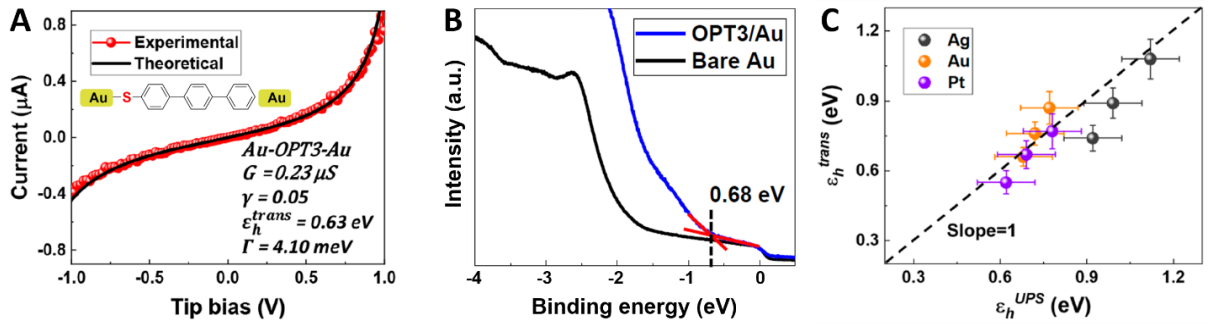

Figure 5. (A) A typical experimental I-V curve and the corresponding SLM fit for an Au-OPT3-Au CP-AFM molecular junction. (B) The UPS spectra of bare gold and a SAM of OPT3 on gold. The two intersecting red lines indicate the onset energy of HOMO relative to the Fermi level (that is, ε_h^{UPS}). (C) Correlation of ε_h^{trans} with ε_h^{UPS} for OPTn (n = 1-3) molecular junctions with Ag, Au, and Pt contacts. Adapted with permission from Ref. 55. Copyright 2019 American Chemical Society.

We distinguish ε_h^{trans}, which is the ε_h determined by SLM fits to *I-V* data ("trans" is short for "electrical transport"), from ε_h^{UPS} determined by UPS. **Figure 5A** shows typical *I-V* data and an SLM fit for a molecular junction based on an oligophenylene thiol (OPT3) SAM; here ε_h^{trans}= 0.63 ± 0.1 eV.[55] **Figure 5B** shows the UPS spectrum and extraction of ε_h^{UPS}.[55] **Figure 5C** displays a correlation of ε_h^{trans} vs ε_h^{UPS} data obtained from many similar measurements based on OPT1, OPT2, and OPT3 SAMs.[55] The close correspondence of the data to the black dashed line (slope = 1) establishes that ε_h^{trans} and ε_h^{UPS} are in good agreement, which provides important support for the validity of the SLM analysis. We have obtained similar agreement for OPD SAMs,

oligophenylene dimethanethiol (OPDM) SAMs, alkyl thiol SAMs, and SAMs of substituted oligophenylene ethynylenes (OPEs).[54–57]

We note that while agreement between the two techniques is gratifying, exact agreement between ε_h^{trans} and ε_h^{UPS} is not expected. A molecular junction has two metal contacts, whereas the UPS experiment probes a SAM on one metal surface. The close proximity of a metal to the molecule can shift ε_h to smaller values through the well-known image charge effect.[57] That is, a molecule very near a metal surface has a lower ionization energy than the same molecule isolated in the gas phase, because the highly polarizable metal screens the positive charge left when an electron is photo-ejected. The image charge effect is expected to be additive, and thus a molecule sandwiched between *two* metals (as in a junction) can be expected to have a lower ionization energy than a molecule close to only one metal (as in a SAM for UPS experiments).[57] So, one anticipates that there would be systematic differences between ε_h^{trans} and ε_h^{UPS} due to differences in the number of proximal metal electrodes (2 vs. 1). In fact, we have observed that this is the case for a series of substituted OPE molecules.[57] We find in that case that ε_h^{trans} is systematically 80 meV lower than ε_h^{UPS}, which we ascribe to the image charge effect of the second contact. DFT calculations support this interpretation.[57] Note that the magnitude of the image charge effect will be different for each molecular junction, because for example, it depends on molecular size (i.e., the distance between the HOMO center and the metal).

4B. Observation of universality across different molecular junctions. Another important success of the Baldea analysis has been to demonstrate that the *I-V* behavior of different molecular junctions with vastly different conductances can be collapsed onto one universal *I-V* curve with suitable normalization.[45,48] Speaking generally, observation of universality demonstrates that the underlying phenomenon of interest, in this case tunneling conductance, operates by the same mechanism in all the samples. When the universal behavior matches the predictions of a model, it is strong evidence that the model provides the appropriate description. Demonstration of universal behavior requires scaling or non-dimensionalizing the experimental parameters by values that reflect the fundamental metrics of the problem.[45] In the case of tunneling conductance of molecules, we can anticipate that scaling voltages by ε_h/e would be appropriate as ε_h is a fundamental energy scale impacting the voltage dependence of transport in the single-level picture. Recalling that the voltage we refer to as V_c is directly related to ε_h via eq. 9, we can choose to scale all voltages by V_c.[45] That is, normalized voltage $V_R = V/V_c$. We scale currents by I_c, the current at V_c; thus, $I_R = I/I_c$.

Figure 6A illustrates the result of this procedure. Here we have taken ~570 total individual *I-V* traces from a series of 24 different alkyl dithiol (C*n*DT, *n* = 8-11) and oligophenylene dithiol (OPD*n*, *n* = 1-4) junctions between Ag, Au, and Pt contacts, and we have divided all voltages by the individual V_c values for each trace.[45] We have correspondingly divided all currents by I_c, the current at $V = V_c$ for each trace. Despite the fact that the low bias conductances *G* for the C*n*DT and OPD*n* junctions *vary by 5 orders of magnitude*, one can see that in the resulting plot of I_R *vs* V_R, all ~570 traces have collapsed into one well defined trend. Furthermore, we have added the red curve that corresponds to the prediction of I_R *vs* V_R from the SLM, i.e., eq. 10 below[45]:

$$I_R = 2V_R/(3 - V_R^2) \qquad (10)$$

In addition, as depicted in **Figure 6B**, the predicted red curve fits the averaged I_R *vs* V_R data very well for all 24 molecular junctions. **Figure 6** thus says that all these molecular junctions behave the same way, that they are all described by the same basic transport physics, which is well described by SLM. What is different for each junction is the specific ε_h and Γ values due to differences in the junction electronic structures. However, the physics of transport is captured by the SLM, so that when suitably normalized, all the data fall on a single universal curve.

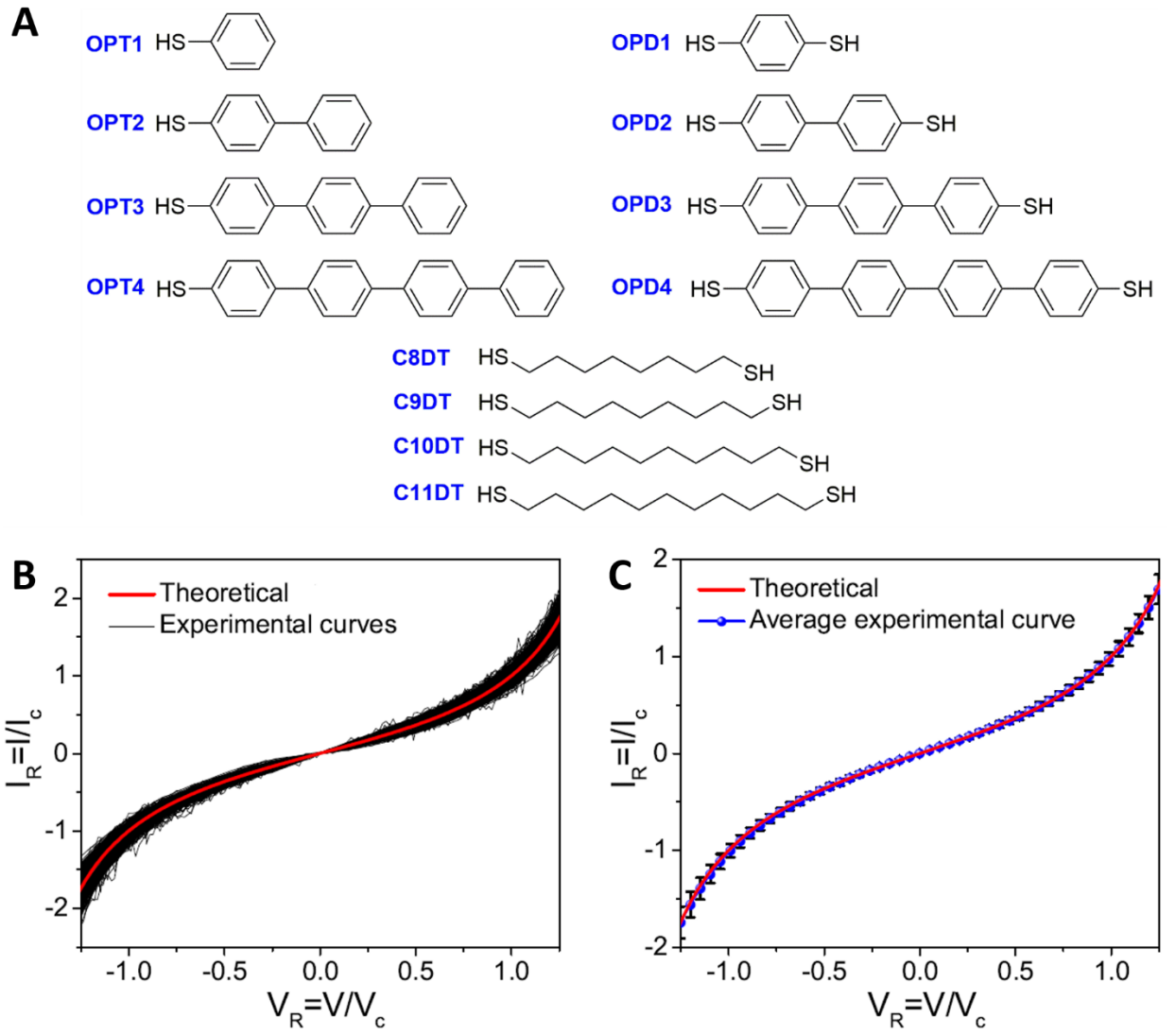

Figure 6. (A) Molecular structures of OPT*n* (*n* = 1-4), OPD*n* (*n* = 1-4), and C*n*DT (*n* = 8-11) (B) The theoretical universal curve of Equation 8 (red) plotted along with ~570 experimental I_R–V_R traces (black) measured for a series of 24 different C*n*DT (*n* = 8-11) and OPD*n* (*n* = 1-4) molecular junctions with Ag, Au, and Pt contacts. (C) Comparison of the theoretical universal curve (red) and the statistical average of ~570 experimental curves analyzed (blue). Error bars (black) represent standard deviations. Reproduced from Ref. 45 with permission from the Royal Society of Chemistry.

4C. Comparison of ε_h, Γ, and γ values to understand connections between junction architecture, electronic structure, and tunneling conductance. The findings just described in sections 4A and 4B solidify the validity of the Baldea SLM model for quantitative analysis of simple molecular junctions. This in turn opens the door to application of the Baldea SLM to extract ε_h, Γ, and γ values from *I-V* data for a variety of molecular systems, bearing in mind the underlying assumptions of this model. **Table 1** shows example data from our laboratory for OPT*n* and OPD*n* SAMs contacted by Ag, Au, and Pt metals using the CP-AFM platform.[47,55] UPS measurements of ε_h and the work function Φ_{SAM}^{UPS} for the SAM-coated metals are also included. Extensive tabulation of electronic structure metrics as a function of junction architecture is currently rare in molecular electronics, but it allows a number of important and insightful observations.

Focusing first on ε_h, we see that ε_h^{trans} and ε_h^{UPS} are in good agreement across all OPT*n* and OPD*n* molecules and all contact metal types, providing confidence in the analysis, as discussed in section 4A. Importantly, the values of ε_h also indicate that the HOMO (not the LUMO) is the facilitating orbital in all cases because the HOMO-LUMO gaps of these molecules are over 3 eV, and thus the HOMO is closer to E_F.[47]

Further, we can use the data in Table 1, some of which are plotted in **Figure 7**, to demonstrate the impact of molecular length (*n*) and contact type (work function, Φ) on key parameters. For example, **Figure 7A** shows that *G* decreases strongly, by orders of magnitude, with molecular length for OPDn, irrespective of the type of contact metal (Ag, Au, or Pt). The corresponding dependencies of ε_h and Γ on molecular length are displayed in **Figures 7C** and **7E**. We see that ε_h decreases as molecular length increases, as can be expected for conjugated molecules, where we know that the HOMO-LUMO gap is a strong function of length. However, the trend of decreasing ε_h with molecular length would seem to imply an *increase* in low bias conductance *G* with length (see Equation 4, HOMO is getting closer to E_F), which is in contradiction to our observation in **Fgure 7A**; the trend in *G* does not match the trend in ε_h. Rather, the sharp decrease in *G* with length better matches the trend in Γ. As shown in **Figure 7E** and **Table 1**, Γ drops by a factor of 8, from 142 meV to 18 meV, for the OPD1-3 series, whereas ε_h only changes by ~17%. Thus, an important conclusion for the OPD*n* system is that the length dependence of *G* primarily reflects the strong length dependence of Γ.

We also discern from **Table 1** and **Figure 7** that *G*, ε_h, and Γ depend on the choice of metal. In fact, *G* increases by over two orders of magnitude as the contact work function Φ increases from 4.25 eV (Ag) to 5.65 eV (Pt), **Figure 7B**. The cause of this increase is again found by looking at the trends in ε_h and Γ. In **Figure 7D** we see that ε_h decreases as the contact work function increases. This is expected, because one would anticipate that a high work function metal should be better aligned to the HOMO of a molecule than a low work function metal. However, close inspection of **Figure 7D** shows that while the work function changes by 1.4 eV from Ag to Pt, the change in ε_h is only ~0.25 eV (~30%)! That is, ε_h is only weakly dependent on Φ. This weak dependence is known at "Fermi level pinning" and it was one of the important discoveries using the CP-AFM platform.[47,54,55,58] The reason for Fermi level pinning is increasing polarization of the C-S bond as

Φ increases,[43,50,59] but a detailed discussion of this effect is beyond our current scope. In contrast, **Figure 7F** shows that Γ depends strongly on Φ. For the OPD3 molecule, for example, Γ ranges from 6.8 meV for Ag contacts, to 18 meV for Au contacts, to 40 meV for Pt contacts. Because G is proportional to Γ^2/ε_h^2 (Equation 4), this factor of 6 difference from Ag to Pt contacts predicts an increase in G of 36× for Pt relative to Ag contacts! The actual increase is 79-fold which reflects that ε_h^{trans} decreases from 0.73 eV to 0.49 eV for Ag vs Pt contacts, producing an additional factor of $(0.73/0.49)^2 = 2.2$, i.e. $G_{Pt}/G_{Ag} = 36 \times 2.2 = 79$. Overall, we can conclude that because of Fermi level pinning the metal contact dependence of G primarily reflects the dependence of Γ on Φ, not ε_h.

Table 1. Key electronic structure parameters, including the energy offsets ε_h^{trans} and ε_h^{UPS}, low-bias conductance G, average coupling Γ, orbital shift factor γ, and work function of the SAM-coated substrate measured by UPS Φ_{SAM}^{UPS}.[a] Adapted with permission from Ref. 55. Copyright 2019 American Chemical Society.

metal	quantity	OPT1	OPT2	OPT3	OPD1	OPD2	OPD3
Ag	ε_h^{trans}	1.08	0.89	0.74	1.00	0.87	0.73
	ε_h^{UPS}	1.12	0.99	0.92	0.83	0.80	0.79
	G	2.34×10^{-7}	2.43×10^{-8}	1.90×10^{-9}	1.20×10^{-5}	3.09×10^{-6}	5.34×10^{-7}
	Γ	7.14	1.88	0.44	43.94	19.45	6.82
	γ	0.023	0.029	0.038	0	0.004	−0.005
	Φ_{SAM}^{UPS}	3.84	3.96	4.03	4.84	4.93	4.89
Au	ε_h^{trans}	0.87	0.76	0.66	0.87	0.73	0.56
	ε_h^{UPS}	0.77	0.72	0.68	0.82	0.74	0.68
	G	1.89×10^{-5}	2.65×10^{-6}	5.18×10^{-7}	1.65×10^{-4}	3.73×10^{-5}	6.65×10^{-6}
	Γ	52.65	16.82	4.52	141.65	56.57	18.34
	γ	0.036	0.037	0.055	0.004	−0.005	−0.003
	Φ_{SAM}^{UPS}	4.72	4.24	4.11	4.72	4.72	4.80
Pt	ε_h^{trans}	0.77	0.67	0.56	0.75	0.63	0.49
	ε_h^{UPS}	0.78	0.69	0.62	0.81	0.72	0.60
	G	8.47×10^{-5}	8.77×10^{-6}	8.55×10^{-7}	1.11×10^{-3}	1.88×10^{-4}	4.17×10^{-5}
	Γ	96.30	27.00	6.98	317.63	109.79	40.14
	γ	0.034	0.033	0.030	−0.005	0	−0.012
	Φ_{SAM}^{UPS}	4.52	4.48	4.37	4.81	4.84	4.77

[a] Units: ε_h in eV, G in S, Γ in meV obtained from eq. 5 by assuming $N = 70$ molecules for OPTn and $N = 80$ molecules for OPDn according to the Maugis-Dugdale (MD) model of contact mechanics, Φ in eV. The UPS data (Φ_{SAM}^{UPS} and ε_h^{UPS}) have an error of ±0.1 eV. Typical relative standard deviations for ε_h^{trans}, G, and Γ are ~5-10%, ~10-25%, and ~10-30%, respectively. More details concerning the error values can be found in Refs. 47, 52, and 55.

One can ask, why does Γ depend on the choice of metal? As Γ represents the degree of metal-molecule coupling (in addition to molecule-molecule coupling), deeper understanding will likely require quantum chemical calculations. However, we have observed that there is a high degree of

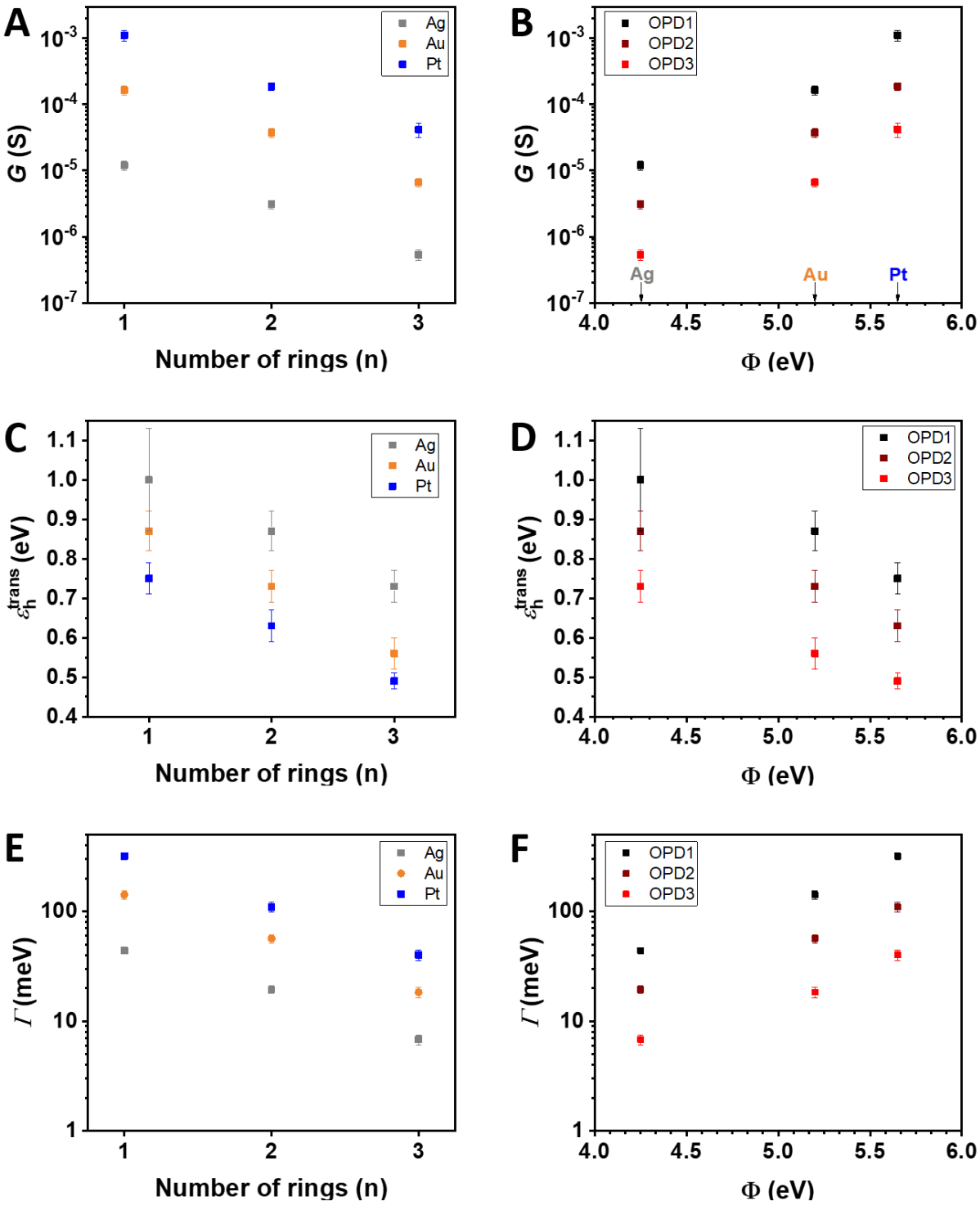

Figure 7. *G* as a function of (A) number of rings (*n*) and (B) bare electrode work function Φ for OPD1-3 CP-AFM molecular junctions with Ag, Au, and Pt contacts. (C) ε_h^{trans} as a function of number of rings (*n*) and (D) bare electrode work function Φ for OPD1-3 CP-AFM molecular junctions with Ag, Au, and Pt contacts. *Γ* as a function of (E) number of rings (*n*) and (F) bare electrode work function Φ for OPD1-3 CP-AFM molecular junctions with Ag, Au, and Pt contacts. Error bars represent standard deviations. Note some scales are linear and some are logarithmic. Adapted with permission from Ref. 47. Copyright 2015 American Chemical Society.

correlation between the interfacial bond dipole in the OPT*n* and OPD*n* systems (which is measured by the work function shift $\Delta\Phi$ of the metal) and Γ. The greater the metal-to-molecule charge transfer on bonding, the greater Γ appears to be. The correlation of Γ and $\Delta\Phi$ is intriguing; it is not in itself an explanation for the dependence of Γ on metal type (correlation is not causation), but it does provide an intriguing direction for further inquiry via quantum chemistry.

So far, our discussion has focused on OPD*n* molecules, not the monothiols OPT*n*. However, inspection of Table 1 shows that for each molecular length (*n* value), the conductance of the OPD*n* molecules is significantly greater than the corresponding OPT*n* molecules. This difference reflects the formation of two metal-S chemical contacts in the OPD*n* case vs one chemical contact in the OPTn case. Indeed, one can see in Table 1 that the electronic coupling Γ is systematically much greater for OPD*n* molecules vs OPT*n*. The general conclusion is that chemical contacts result in greater electronic coupling than physical contacts, which is certainly appreciated in the community,[55,58,60–65] but with our analytical model we can quantify it.

Finally, comparison of the γ values in **Table 1** shows that in all cases γ is rather small, typically just a few percent or tenths of a percent. That is, OPT*n* and OPD*n* junctions do not exhibit significant shifting of the HOMO energy upon application of a bias. Recall that $\gamma = 0.05$ (for OPT3 between Au contacts) means that application of a 1 V bias (a large value) produces only a 50 meV shift in ε_h. Still the γ values for the OPD*n* molecules are always systematically smaller than for OPT*n*. This is consistent with expectations based on the symmetries of the two types of molecules. OPT*n* is less symmetric, with only one thiol group and thus the HOMO "center of gravity" is closer to the thiol side of the molecule, which results in larger γ values. The fact that $\gamma > 0$ for OPT*n* means the HOMO energy weakly tracks the substrate electrode, which is consistent with the slight spatial displacement of the HOMO toward the thiol side of the molecule.[51]

One can see from this discussion that the collection of electronic structure metrics shown in Table 1, which come straightforwardly from the SLM analysis, facilitates identification of many important trends and structure-property relationships for molecular junctions. SLM does not by itself provide complete answers for some questions, such as how Γ depends on metal work function, but the ability to extract ε_h, Γ, and γ quickly from the *I-V* data for a wide variety of junction structures provides an important first step in understanding where to look for deeper explanations using quantum chemical calculations.

5. Challenges

The foregoing overview makes the case that the Baldea version of the single level model advances the field of molecular electronics by conveniently and efficiently enhancing quantitative analysis, specifically the quantitative connection between transport behavior and electronic structure of molecular junctions. However, it should be clear that this model applies only to the simplest of molecular junctions where transport is well described by off-resonant, single-step tunneling. It must only be used in situations where the core assumptions underlying its derivation apply.

One specific phenomenon that SLM (eqs. 3 or 8) does not capture transparently is the phenomenon of quantum interference in tunneling transport. Quantum interference requires tunneling to be facilitated by two or more orbitals that have different phase relationships or nodal structures.[66,67] The quantum interference of orbitals, constructive or destructive, can have significant impact on total junction transmission. By assuming that transport is dominated by only one orbital, the SLM seemingly omits this effect.

However, in off-resonant molecular junctions, quantum interference is generally most important for low junction biases where transport is occurring at or near the equilibrium Fermi level. At low biases, transport occurs through the overlapping "Lorentzian tails" of the HOMO and HOMO−1 (or LUMO and LUMO+1), for example. Many DFT calculations indicate that quantum interference can be important in this case.[41,42] But as the junction bias voltage increases, the orbital closest in energy to the Fermi level – say the HOMO – will dominate. This is especially true when the junction orbitals are significantly separated in energy from each other, with separations on the order of ε_h itself. Thus, the single-level approximation becomes more correct as bias increases. Because in the SLM analysis ε_h is derived from the higher bias portions of the *I-V* curve, accurate values can be obtained, as we have seen above. This means that the effects of quantum interference on the SLM analysis appear not in ε_h, but in the low bias conductance G and by extension in Γ (see eq. 5). In junctions where quantum interference is important, the SLM model captures the effect in Γ. In such a case, Γ is no longer the electronic coupling of just the HOMO (or LUMO) to the electrodes, but it is a composite Γ reflecting all the orbitals that contribute to $T(\varepsilon)$ around the Fermi level. So, in this respect, the SLM *does* reflect the quantum interference phenomenon; it gets incorporated into the Γ value.

There are other practical challenges to broader implementation of SLM analysis in the molecular electronics community. One is that in order to extract Γ from the low bias conductance G, one needs to know the number of molecules N in the junction. For large area junctions, such as those based on eutectic-GaIn (EGaIn) contacts, N is not accurately known.[68] Still, even in these systems extraction of ε_h should be possible from the shape of the *I-V* curves. For single-molecule junctions where $N = 1$, the SLM can be applied to extract ε_h, Γ, and γ. However, in the literature often only low bias G values are measured and full *I-V* curves are not always reported for single-molecule junctions. This problem seems readily addressable by the community and we believe that the quantitative foundation of molecular electronics will be enhanced by increased reporting of electronic structure metrics.

6. Conclusion and Future Outlook

Our goal in this Perspective has been to show that an analytical model for tunneling transport in molecular junctions correctly captures the *I-V* behavior for many simple cases, and furthermore that this allows convenient extraction and tabulation of electronic structure parameters. In our view, the benefits of the SLM (the Baldea version in particular) are that it provides transparency regarding the essential physics in many molecular junctions, that it is readily accessible to the experimentalist, and that it returns values for parameters that can then be easily compared for different junctions as a function of molecular structure, contact chemistry, and choice of metals,

for example. It is our perspective that the development of molecular electronics as a vital sub-discipline of chemistry will be enhanced by quantitative analysis, and the model discussed here provides a convenient approach to achieve that goal.

Acknowledgements
CDF thanks the US National Science Foundation (NSF) for its long term support of this work (current award CHE-2304763). CDF also thanks Ioan Baldea for his theoretical insights, thought-provoking discussions, and productive collaboration over many years.

References

1 M. A. Reed, C. Zhou, C. J. Muller, T. P. Burgin and J. M. Tour, Conductance of a Molecular Junction, *Science*, 1997, **278**, 252–254.
2 X. D. Cui, A. Primak, X. Zarate, J. Tomfohr, O. F. Sankey, A. L. Moore, T. A. Moore, D. Gust, G. Harris and S. M. Lindsay, Reproducible Measurement of Single-Molecule Conductivity, *Science*, 2001, **294**, 571–574.
3 B. Xu and N. J. Tao, Measurement of Single-Molecule Resistance by Repeated Formation of Molecular Junctions, *Science*, 2003, **301**, 1221–1223.
4 T. Albrecht, A. Guckian, J. Ulstrup and J. G. Vos, Transistor-like Behavior of Transition Metal Complexes, *Nano Lett.*, 2005, **5**, 1451–1455.
5 X. Li, J. He, J. Hihath, B. Xu, S. M. Lindsay and N. Tao, Conductance of single alkanedithiols: conduction mechanism and effect of molecule-electrode contacts., *J. Am. Chem. Soc.*, 2006, **128**, 2135–41.
6 R. C. Chiechi, E. A. Weiss, M. D. Dickey and G. M. Whitesides, Eutectic Gallium–Indium (EGaIn): A Moldable Liquid Metal for Electrical Characterization of Self-Assembled Monolayers, *Angew. Chemie*, 2008, **120**, 148–150.
7 S. Ho Choi, B. Kim and C. D. Frisbie, Electrical Resistance of Long Conjugated Molecular Wires, *Science*, 2008, **320**, 1482–1486.
8 I. Ron, L. Sepunaru, S. Itzhakov, T. Belenkova, N. Friedman, I. Pecht, M. Sheves and D. Cahen, Proteins as Electronic Materials: Electron Transport through Solid-State Protein Monolayer Junctions, *J. Am. Chem. Soc.*, 2010, **132**, 4131–4140.
9 C. Jia, A. Migliore, N. Xin, S. Huang, J. Wang, Q. Yang, S. Wang, H. Chen, D. Wang, B. Feng, Z. Liu, G. Zhang, D.-H. Qu, H. Tian, M. A. Ratner, H. Q. Xu, A. Nitzan and X. Guo, Covalently bonded single-molecule junctions with stable and reversible photoswitched conductivity, *Science*, 2016, **352**, 1443–1445.
10 B. Han, Y. Li, X. Ji, X. Song, S. Ding, B. Li, H. Khalid, Y. Zhang, X. Xu, L. Tian, H. Dong, X. Yu and W. Hu, Systematic Modulation of Charge Transport in Molecular Devices through Facile Control of Molecule–Electrode Coupling Using a Double Self-Assembled Monolayer Nanowire Junction, *J. Am. Chem. Soc.*, 2020, **142**, 9708–9717.
11 C. A. Nijhuis, Z. Zhang, F. Adoah, C. Nickle, S. K. Karuppannan, L. Wang, L. Jiang, A. Tadich, B. Cowie, T. Salim, D. Qi, D. Thompson and E. Del Barco, Control over Molecular Orbital Gating and Marcus Inverted Charge Transport in Molecular Junctions with Conjugated Molecular Wires, *Adv. Electron. Mater.*, 2023, **9**, 2200637.
12 I. Díez-Pérez, J. Hihath, Y. Lee, L. Yu, L. Adamska, M. A. Kozhushner, I. I. Oleynik and N. Tao, Rectification and stability of a single molecular diode with controlled orientation, *Nat. Chem. 2009 18*, 2009, **1**, 635–641.

13 B. Capozzi, J. Xia, O. Adak, E. J. Dell, Z. F. Liu, J. C. Taylor, J. B. Neaton, L. M. Campos and L. Venkataraman, Single-molecule diodes with high rectification ratios through environmental control, *Nat. Nanotechnol.*, 2015, **10**, 522–527.
14 Q. van Nguyen, P. Martin, D. Frath, M. L. Della Rocca, F. Lafolet, C. Barraud, P. Lafarge, V. Mukundan, D. James, R. L. McCreery and J.-C. Lacroix, Control of Rectification in Molecular Junctions: Contact Effects and Molecular Signature, *J. Am. Chem. Soc.*, 2017, **139**, 11913–11922.
15 X. Chen, M. Roemer, L. Yuan, W. Du, D. Thompson, E. del Barco and C. A. Nijhuis, Molecular diodes with rectification ratios exceeding 105 driven by electrostatic interactions, *Nat. Nanotechnol.*, 2017, **12**, 797–803.
16 A. J. Kronemeijer, H. B. Akkerman, T. Kudernac, B. J. Van Wees, B. L. Feringa, P. W. M. Blom and B. De Boer, Reversible conductance switching in molecular devices, *Adv. Mater.*, 2008, **20**, 1467–1473.
17 S. Y. Quek, M. Kamenetska, M. L. Steigerwald, H. J. Choi, S. G. Louie, M. S. Hybertsen, J. B. Neaton and L. Venkataraman, Mechanically controlled binary conductance switching of a single-molecule junction, *Nat. Nanotechnol.*, 2009, **4**, 230–234.
18 T. A. Su, H. Li, M. L. Steigerwald, L. Venkataraman and C. Nuckolls, Stereoelectronic switching in single-molecule junctions, *Nat. Chem.*, 2015, **7**, 215–220.
19 M. A. Mangold, M. Calame, M. Mayor and A. W. Holleitner, Resonant Photoconductance of Molecular Junctions Formed in Gold Nanoparticle Arrays, *J. Am. Chem. Soc.*, 2011, **133**, 12185–12191.
20 J. Zhou, K. Wang, B. Xu and Y. Dubi, Photoconductance from Exciton Binding in Molecular Junctions, *J. Am. Chem. Soc.*, 2018, **140**, 70–73.
21 Q. Zou, X. Chen, Y. Zhou, X. Jin, Z. Zhang, J. Qiu, R. Wang, W. Hong, J. Su, D. H. Qu and H. Tian, Photoconductance from the Bent-to-Planar Photocycle between Ground and Excited States in Single-Molecule Junctions, *J. Am. Chem. Soc.*, 2022, **144**, 10042–10052.
22 S. Schmaus, A. Bagrets, Y. Nahas, T. K. Yamada, A. Bork, M. Bowen, E. Beaurepaire, F. Evers and W. Wulfhekel, Giant magnetoresistance through a single molecule, *Nat. Nanotechnol.*, 2011, **6**, 185–189.
23 Z. Xie, S. Shi, F. Liu, D. L. Smith, P. P. Ruden and C. D. Frisbie, Large Magnetoresistance at Room Temperature in Organic Molecular Tunnel Junctions with Nonmagnetic Electrodes, *ACS Nano*, 2016, **10**, 8571–8577.
24 K. Yang, H. Chen, T. Pope, Y. Hu, L. Liu, D. Wang, L. Tao, W. Xiao, X. Fei, Y.-Y. Zhang, H.-G. Luo, S. Du, T. Xiang, W. A. Hofer and H.-J. Gao, Tunable giant magnetoresistance in a single-molecule junction, *Nat. Commun.*, 2019, **10**, 3599.
25 J. M. Chen, J., Reed, M. A., Rawlett, A. M., Tour, Large On-Off Ratios and Negative Differential Resistance in a Molecular Electronic Device, *Science*, 1999, **286**, 1550–1552.
26 N. P. Guisinger, M. E. Greene, R. Basu, A. S. Baluch and M. C. Hersam, Room Temperature Negative Differential Resistance through Individual Organic Molecules on Silicon Surfaces, *Nano Lett.*, 2004, **4**, 55–59.
27 M. L. Perrin, R. Frisenda, M. Koole, J. S. Seldenthuis, J. A. C. Gil, H. Valkenier, J. C. Hummelen, N. Renaud, F. C. Grozema, J. M. Thijssen, D. Dulić and H. S. J. Van Der Zant, Large negative differential conductance in single-molecule break junctions, *Nat. Nanotechnol*, 2014, **9**, 830–834.
28 D. Xiang, X. Wang, C. Jia, T. Lee and X. Guo, Molecular-Scale Electronics: From Concept to Function, *Chem. Rev.*, 2016, **116**, 4318–4440.

29 A. Vilan, D. Aswal and D. Cahen, Large-Area, Ensemble Molecular Electronics: Motivation and Challenges, *Chem. Rev.*, 2017, **117**, 4248–4286.
30 H. Jeong, D. Kim, D. Xiang and T. Lee, High-Yield Functional Molecular Electronic Devices, *ACS Nano*, 2017, **11**, 6511–6548.
31 P. T. Mathew and F. Fang, Advances in Molecular Electronics: A Brief Review, *Engineering*, 2018, **4**, 760–771.
32 H. Chen and J. Fraser Stoddart, From molecular to supramolecular electronics, *Nat. Rev. Mater.*, 2021, **6**, 804–828.
33 R. J. Nichols, Molecular electronics at electrode–electrolyte interfaces, *Curr. Opin. Electrochem.*, 2021, **25**, 100650.
34 M. R. Bryce, A review of functional linear carbon chains (oligoynes, polyynes, cumulenes) and their applications as molecular wires in molecular electronics and optoelectronics, *J. Mater. Chem. C*, 2021, **9**, 10524–10546.
35 I. Bâldea, Ambipolar transition voltage spectroscopy: Analytical results and experimental agreement, *Phys. Rev. B*, 2012, **85**, 035442.
36 N. J. Tao, Electron transport in molecular junctions., *Nat. Nanotechnol.*, 2006, **1**, 173–81.
37 S. Datta, *Quantum Transport: Atom to Transistor*, Cambridge University Press, 2005.
38 A. Vilan, D. Cahen and E. Kraisler, Rethinking Transition Voltage Spectroscopy within a Generic Taylor Expansion View, *ACS Nano*, 2013, **7**, 695–706.
39 X. Song, B. Han, X. Yu and W. Hu, The analysis of charge transport mechanism in molecular junctions based on current-voltage characteristics, *Chem. Phys.*, 2020, **528**, 110514.
40 Z. Bihary and M. A. Ratner, *Adv. Quantum Chem.*, 2005, **48**, 23–34.
41 G. C. Solomon, D. Q. Andrews, R. H. Goldsmith, T. Hansen, M. R. Wasielewski, R. P. Van Duyne and M. A. Ratner, Quantum Interference in Acyclic Systems: Conductance of Cross-Conjugated Molecules, *J. Am. Chem. Soc.*, 2008, **130**, 17301–17308.
42 D. Q. Andrews, G. C. Solomon, R. H. Goldsmith, T. Hansen, M. R. Wasielewski, R. P. Van Duyne and M. A. Ratner, Quantum interference: The structural dependence of electron transmission through model systems and cross-conjugated molecules, *J. Phys. Chem. C*, 2008, **112**, 16991–16998.
43 C. Van Dyck, V. Geskin, A. J. Kronemeijer, D. M. de Leeuw and J. Cornil, Impact of derivatization on electron transmission through dithienylethene-based photoswitches in molecular junctions, *Phys. Chem. Chem. Phys.*, 2013, **15**, 4392.
44 P. Darancet, J. R. Widawsky, H. J. Choi, L. Venkataraman and J. B. Neaton, Quantitative Current–Voltage Characteristics in Molecular Junctions from First Principles, *Nano Lett.*, 2012, **12**, 6250–6254.
45 I. Bâldea, Z. Xie and C. D. Frisbie, Uncovering a law of corresponding states for electron tunneling in molecular junctions, *Nanoscale*, 2015, **7**, 10465–10471.
46 E. Scheer and J. C. Cuevas, *Molecular Electronics: An Introduction to Theory and Experiment*, World Scientific, 2nd ed., 2017.
47 Z. Xie, I. Bâldea, C. E. Smith, Y. Wu and C. D. Frisbie, Experimental and Theoretical Analysis of Nanotransport in Oligophenylene Dithiol Junctions as a Function of Molecular Length and Contact Work Function, *ACS Nano*, 2015, **9**, 8022–8036.
48 Z. Xie, I. Bâldea, S. Oram, C. E. Smith and C. D. Frisbie, Effect of Heteroatom Substitution on Transport in Alkanedithiol-Based Molecular Tunnel Junctions: Evidence for Universal Behavior, *ACS Nano*, 2017, **11**, 569–578.

49 Z. Xie, I. Bâldea and C. D. Frisbie, Why one can expect large rectification in molecular junctions based on alkane monothiols and why rectification is so modest, *Chem. Sci.*, 2018, **9**, 4456–4467.

50 S. Rodriguez-Gonzalez, Z. Xie, O. Galangau, P. Selvanathan, L. Norel, C. Van Dyck, K. Costuas, C. D. Frisbie, S. Rigaut and J. Cornil, HOMO Level Pinning in Molecular Junctions: Joint Theoretical and Experimental Evidence, *J. Phys. Chem. Lett.*, 2018, **9**, 2394–2403.

51 Z. Xie, I. Bâldea, Q. Van Nguyen and C. D. Frisbie, Quantitative analysis of weak current rectification in molecular tunnel junctions subject to mechanical deformation reveals two different rectification mechanisms for oligophenylene thiols versus alkane thiols, *Nanoscale*, 2021, **13**, 16755–16768.

52 Z. Xie, I. Bâldea, A. T. Demissie, C. E. Smith, Y. Wu, G. Haugstad and C. D. Frisbie, Exceptionally Small Statistical Variations in the Transport Properties of Metal–Molecule–Metal Junctions Composed of 80 Oligophenylene Dithiol Molecules, *J. Am. Chem. Soc.*, 2017, **139**, 5696–5699.

53 J. M. Beebe, B. Kim, C. D. Frisbie and J. G. Kushmerick, Measuring Relative Barrier Heights in Molecular Electronic Junctions with Transition Voltage Spectroscopy, *ACS Nano*, 2008, **2**, 827–832.

54 Z. Xie, I. Bâldea and C. D. Frisbie, Energy Level Alignment in Molecular Tunnel Junctions by Transport and Spectroscopy: Self-Consistency for the Case of Alkyl Thiols and Dithiols on Ag, Au, and Pt Electrodes, *J. Am. Chem. Soc.*, 2019, **141**, 18182–18192.

55 Z. Xie, I. Bâldea and C. D. Frisbie, Determination of Energy-Level Alignment in Molecular Tunnel Junctions by Transport and Spectroscopy: Self-Consistency for the Case of Oligophenylene Thiols and Dithiols on Ag, Au, and Pt Electrodes, *J. Am. Chem. Soc.*, 2019, **141**, 3670–3681.

56 Q. Van Nguyen, Z. Xie and C. D. Frisbie, Quantifying Molecular Structure-Tunneling Conductance Relationships: Oligophenylene Dimethanethiol vs Oligophenylene Dithiol Molecular Junctions, *J. Phys. Chem. C*, 2021, **125**, 4292–4298.

57 Z. Xie, V. Diez Cabanes, Q. Van Nguyen, S. Rodriguez-Gonzalez, L. Norel, O. Galangau, S. Rigaut, J. Cornil and C. D. Frisbie, Quantifying Image Charge Effects in Molecular Tunnel Junctions Based on Self-Assembled Monolayers of Substituted Oligophenylene Ethynylene Dithiols, *ACS Appl. Mater. Interfaces*, 2021, **13**, 56404–56412.

58 B. Kim, S. H. Choi, X.-Y. Zhu and C. D. Frisbie, Molecular tunnel junctions based on π-conjugated oligoacene thiols and dithiols between Ag, Au, and Pt contacts: effect of surface linking group and metal work function., *J. Am. Chem. Soc.*, 2011, **133**, 19864–77.

59 G. Heimel, L. Romaner, E. Zojer and J.-L. Brédas, Toward Control of the Metal−Organic Interfacial Electronic Structure in Molecular Electronics: A First-Principles Study on Self-Assembled Monolayers of π-Conjugated Molecules on Noble Metals, *Nano Lett.*, 2007, **7**, 932–940.

60 G. Wang, T.-W. Kim, H. Lee and T. Lee, Influence of metal-molecule contacts on decay coefficients and specific contact resistances in molecular junctions, *Phys. Rev. B*, 2007, **76**, 205320.

61 G. Wang, T. W. Kim, Y. H. Jang and T. Lee, Effects of metal-molecule contact and molecular structure on molecular electronic conduction in nonresonant tunneling regime: Alkyl versus conjugated molecules, *J. Phys. Chem. C*, 2008, **112**, 13010–13016.

62 A. Salomon, D. Cahen, S. Lindsay, J. Tomfohr, V. B. Engelkes and C. D. Frisbie,

Comparison of Electronic Transport Measurements on Organic Molecules, *Adv. Mater.*, 2003, **15**, 1881–1890.
63 J. G. Kushmerick, Metal-molecule contacts, *Mater. Today*, 2005, **8**, 26–30.
64 H. B. Akkerman and B. De Boer, Electrical conduction through single molecules and self-assembled monolayers, *J. Phys. Condens. Matter*, 2007, **20**, 013001.
65 A. Tan, J. Balachandran, S. Sadat, V. Gavini, B. D. Dunietz, S.-Y. Jang and P. Reddy, Effect of Length and Contact Chemistry on the Electronic Structure and Thermoelectric Properties of Molecular Junctions, *J. Am. Chem. Soc.*, 2011, **133**, 8838–8841.
66 G. C. Solomon, D. Q. Andrews, T. Hansen, R. H. Goldsmith, M. R. Wasielewski, R. P. Van Duyne and M. A. Ratner, Understanding quantum interference in coherent molecular conduction, *J. Chem. Phys.*, 2008, **129**, 054701.
67 J. Liu, X. Huang, F. Wang and W. Hong, Quantum Interference Effects in Charge Transport through Single-Molecule Junctions: Detection, Manipulation, and Application, *Acc. Chem. Res.*, 2019, **52**, 151–160.
68 C. A. Nijhuis, W. F. Reus, J. R. Barber and G. M. Whitesides, Comparison of SAM-Based Junctions with Ga 2 O 3 /EGaIn Top Electrodes to Other Large-Area Tunneling Junctions, *J. Phys. Chem. C*, 2012, **116**, 14139–14150.